Model for passive mode locking in semiconductor lasers

Andrei G. Vladimirov*
Weierstrass Institute for Applied Analysis and Stochastics, Mohrenstrasse 39, D-10117 Berlin, Germany

Dmitry Turaev†
Ben Gurion University, P. O. Box 653, 84105 Be'er Sheva, Israel

(Received 19 November 2004; revised manuscript received 11 May 2005; published 12 September 2005)

We derive and study a model describing passive mode locking—a set of differential equations with time delay. Unlike classical mode locking models based on the Haus master equation, this model does not assume small gain and loss per cavity round trip. Therefore, it is valid in a parameter range typical of semiconductor lasers. The limit of a slow saturable absorber is analyzed analytically. Bifurcations responsible for the appearance and breakup of the mode locking regime are studied numerically.

DOI: 10.1103/PhysRevA.72.033808 PACS number(s): 42.60.Fc, 42.65.Sf, 42.60.Gd, 42.65.Pc

INTRODUCTION

Passive mode locking (ML) is a powerful method to generate high-quality short pulses with high repetition rates from different kinds of lasers. In particular, passively and hybrid mode-locked semiconductor lasers are compact, low-cost, reliable, and efficient sources of picosecond and subpicosecond pulses ideal for applications in high-speed communication systems [1]. Due to the small size, large gain coefficient, and fast recovery time of semiconductor material these lasers can produce pulses at very high repetition rates (tens and hundreds of gigahertz). The duration of ML pulses generated by semiconductor lasers is typically much smaller than the semiconductor saturable absorber recovery time. This situation is usually referred to as a ML with slow saturable absorber [2]. The basic physical mechanism responsible for the appearance of passive ML in a laser with slow absorber has been known for a long time: with the arrival of a pulse, the absorbing medium saturates faster than the amplifying one, and, therefore, a short net gain window is opened, ensuring the pulse amplification that is necessary to compensate cavity round-trip losses [3]. However, nonlinear dynamical regimes that can arise in mode-locked lasers and bifurcations of these regimes are still quite poorly understood. We believe that the delay differential model described in this paper could help to fill this gap.

Analytical approaches to describe passive ML with a slow saturable absorber were developed by New and Haus [2,3]. Both of them considered the situation of small gain and loss per cavity round trip. Assuming the absence of spectral filtering New obtained implicit analytical expressions for the stability boundaries of the ML regime in the space of laser parameters. Haus developed a ML model that takes spectral filtering into consideration under a parabolic approximation. He derived analytical expression for the shape of a ML pulse in the limit of small pulse energy, when the intracavity media are weakly saturated. His results were found to be in a good agreement with the experimental data obtained with dye laser [4]. Since then, different modifications of the Haus model have been derived and analyzed; see reviews [5–8] and references therein.

Despite the success of the Haus master equation, its ability to describe adequately real laser systems is questionable in many situations. In particular, typical solid-state lasers with semiconductor saturable absorbers are operated under conditions of almost complete saturation [9], which violates the assumptions underlying Haus' model. Another example is given by semiconductor mode-locked lasers. They typically have high gain and losses per cavity round trip, which invalidates both New and Haus classical models. This is why approaches based on direct numerical simulations of spatially distributed models have been mainly used to study ML in semiconductor lasers (for a review, see Ref. [8]). Although the direct numerical simulations are, in principle, capable to reproduce experimental data, they give only little insight into the physical mechanisms involved.

In this paper we derive and study a delay differential model, announced in [10], which is able to describe ML in the parameter range typical of semiconductor lasers. When deriving this model we do not use the small-gain and -loss, weak-saturation, and infinite-bandwidth approximations. The only essential assumption we adopt is a ring-cavity geometry with unidirectional lasing. Being more general than the classical ML models, our model remains simple enough for a comprehensive bifurcation analysis and allows for a clear physical interpretation. Here we present the results of an analytical study of the delay differential model in the limit of a slow saturable absorber. In particular, we show how models similar to those by New and Haus are derived in the case where the gain and loss per cavity round trip are not small, and discuss the applicability limits of these models. In order to describe bifurcations of the fundamental and multiple ML regimes we perform a numerical analysis of the delay differential model. We find that two main mechanisms are responsible for the onset and breakup of these regimes: the low-frequency Q-switching instability and a sudden chaotization via intermittency. Special attention is paid to the strong and very asymmetric impact of linewidth enhancement factors on ML solutions. Among other results we show that stable ML

*Email address: vladimir@wias-berlin.de
†Email address: turaev@cs.bgu.ac.il

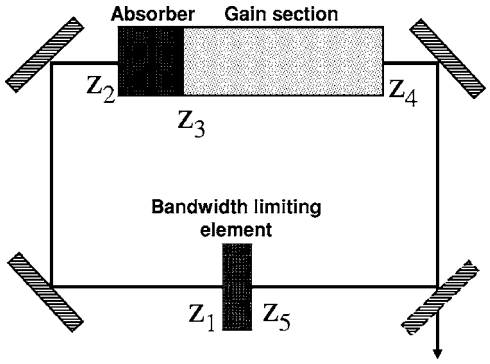

FIG. 1. Schematic representation of a ring passively mode-locked laser. Coordinate z is measured along the cavity axis. Interval $z_2<z<z_3 (z_3<z<z_4)$ corresponds to absorbing (amplifying) section. Spectral filtering element is placed between $z=z_5$ and $z=z_1+L$, where L is the cavity length. Intervals $z_1<z<z_2$ and $z_4<z<z_5$ are filled with passive medium.

pulses with positive net gain at the leading edge can exist in a certain parameter range and investigate the sensitivity of such and other ML solutions to noise.

I. MODEL EQUATIONS

In this section we use the so-called lumped-element method to derive delay differential equations for a ring mode-locked laser. Let us consider the laser shown schematically in Fig. 1. It is assumed that one of the two counterpropagating waves in the laser cavity is suppressed so that the lasing is unidirectional. The laser consists of five sections. Let z be the coordinate along the cavity axis. The first $z_1<z<z_2$ and the fourth $z_4<z<z_5$ sections are passive. The second $z_2<z<z_3$ and the third $z_3<z<z_4$ sections contain saturable absorber and gain medium, respectively. The last, fifth section $z_5<z<z_1+L$ acts as a spectral filter that limits the bandwidth of the laser radiation. Here L is the cavity length. The so-called traveling-wave equations [11,12] governing evolution of the slowly varying electric field envelope $E(t,z)$ in the gain and absorber sections can be written in the form

$$\frac{\partial E(t,z)}{\partial z}+\frac{1}{v}\frac{\partial E(t,z)}{\partial t}=\frac{g_r\Gamma_r}{2}(1-i\alpha_r)[N_r(t,z)-N_r^{tr}]E(t,z), \tag{1}$$

$$\frac{\partial N_r(t,z)}{\partial t}=J_r-\gamma_r N_r(t,z)-vg_r\Gamma_r[N_r(t,z)-N_r^{tr}]|E(t,z)|^2. \tag{2}$$

Here the subscript $r=g$ $(r=q)$ corresponds to the gain (absorber) section. The variables $N_g(z,t)$ and $N_q(z,t)$ describe carrier densities in the gain and absorber sections, respectively. The parameters $N_{g,q}^{tr}$ are the carrier densities evaluated at transparency threshold. The parameter v is the light group velocity which is assumed to be constant and equal in all the five sections. The parameters $\alpha_{g,q}$, $g_{g,q}$, $\Gamma_{g,q}$, and $\gamma_{g,q}$ are, respectively, linewidth enhancement factors, differential gains, transverse modal fill factors, and carrier density relaxation rates in the gain and absorber sections. The parameter J_g describes injection current in the gain section. For the absorber section we have $J_q=0$.

Evolution of the electric field envelope $E(t,z)$ in the passive sections is governed by the equation

$$\frac{\partial E(t,z)}{\partial z}+\frac{1}{v}\frac{\partial E(t,z)}{\partial t}=0. \tag{3}$$

The spectral filtering section describes material gain dispersion together with that of any artificial dispersive elements such as distributed Bragg reflectors. Transformation of the electric field envelope by this section is given by

$$\hat{E}(\omega,z_1+L)=\hat{f}(\omega)\hat{E}(\omega,z_5), \tag{4}$$

where $\hat{E}(\omega,z_5)$ and $\hat{E}(\omega,z_1+L)$ are the Fourier transforms of $E(t,z_5)$ and $E(t,z_1+L)$, respectively. The function $\hat{f}(\omega)$ in Eq. (4) describes the line shape of the bandwidth-limiting element. In a ring cavity the electric field envelope E obeys the periodic boundary condition $E(t,z+L)=E(t,z)$.

After the coordinate change $(t,z)\rightarrow(\tau,\zeta)$, where $\tau=\gamma_q(t-z/v)$ is the retarded time divided by the absorber relaxation time, and $\zeta=z\gamma_q/v$ is the normalized coordinate along the cavity axis, Eqs. (1) and (2) take the following adimensional form:

$$\frac{\partial A(\tau,z)}{\partial\zeta}=\frac{1}{2}(1-i\alpha_{g,q})n_{g,q}(\tau,z)A(\tau,z), \tag{5}$$

$$\frac{\partial n_g(\tau,z)}{\partial\tau}=j_g-\Gamma n_g(\tau,z)-n_g(\tau,z)|A(\tau,z)|^2, \tag{6}$$

$$\frac{\partial n_q(\tau,z)}{\partial\tau}=-j_q-n_q(\tau,z)-sn_q(\tau,z)|A(\tau,z)|^2. \tag{7}$$

Here $A(\tau,\zeta)=E(t,z)\sqrt{vg_g\Gamma_g/\gamma_q}$, $n_{g,q}(\tau,\zeta)=vg_{g,q}\Gamma_{g,q}[N_{g,q}(t,z)-N_{g,q}^{tr}]/\gamma_q$, $j_g=vg_g\Gamma_g(J_g-\gamma_gN_g^{tr})/\gamma_q^2$, $j_q=vg_g\Gamma_gN_q^{tr}/\gamma_q$, and $\Gamma=\gamma_g/\gamma_q$. The parameter $s=(g_q\Gamma_q)/(g_g\Gamma_g)$ is the ratio of the saturation intensities in the gain and absorber sections.

In the new coordinates (τ,ζ) Eq. (3) for the passive sections takes the form

$$\frac{\partial A(\tau,\zeta)}{\partial\zeta}=0. \tag{8}$$

By solving Eqs. (5)–(8) and Eq. (4), the transformation of the electric field amplitude by each of the five laser sections is evaluated. According to Eq. (8), the relations between input and output fields in the two passive sections are

$$A(\tau,\zeta_2)=A(\tau,\zeta_1),\quad A(\tau,\zeta_5)=A(\tau,\zeta_4), \tag{9}$$

where $\zeta_k=z_k\gamma_q/v$ $(k=1,2,3,4,5)$. The transformations of the electric field amplitude by the gain and absorber sections are obtained by the integration of Eq. (5):

$$A(\tau,\zeta_4) = e^{(1-i\alpha_g)G(\tau)/2}A(\tau,\zeta_3),$$

$$A(\tau,\zeta_3) = e^{-(1-i\alpha_q)Q(\tau)/2}A(\tau,\zeta_2). \quad (10)$$

Here the dimensionless quantities $G(\tau)$ and $Q(\tau)$ describe saturable gain and loss introduced by the absorber and gain sections [13,14]. They are given by $G(\tau)=\int_{\zeta_3}^{\zeta_4} n_g(\tau,\zeta)d\zeta$ and $Q(\tau)=-\int_{\zeta_2}^{\zeta_3} n_q(\tau,\zeta)d\zeta$. Integrating Eqs. (6) and (7) over ζ from ζ_3 to ζ_4 and from ζ_2 to ζ_3, respectively, and using the relation $\int_{\zeta_{2,3}}^{\zeta_{3,4}} n_{q,g}(\zeta,\tau)|A(\tau,\zeta)|^2 d\zeta = -|A(\zeta_{3,4},\tau)|^2 + |A(\zeta_{2,3},\tau)|^2$, which follows from Eq. (5), we derive the equations governing the evolution of the saturable gain and loss:

$$\partial_\tau G(\tau) = g_0 - \Gamma G(\tau) - |A(\tau,\zeta_4)|^2 + |A(\tau,\zeta_3)|^2, \quad (11)$$

$$\partial_\tau Q(\tau) = q_0 - Q(\tau) + s|A(\tau,\zeta_3)|^2 - s|A(\tau,\zeta_2)|^2. \quad (12)$$

Here the unsaturated gain (pump) and absorption parameters are defined by $g_0=\int_{\zeta_3}^{\zeta_4} j_g d\zeta$ and $q_0=\int_{\zeta_2}^{\zeta_3} j_q d\zeta$, respectively.

Being rewritten in the time domain, Eq. (4) for the spectral filtering section takes the form

$$A(\tau,\zeta_1+T) = \int_{-\infty}^{\tau} f(\tau-\theta)A(s,\zeta_5)d\theta, \quad (13)$$

where $T=\gamma_q L/v$ is the normalized cold-cavity round-trip time and $f(\tau)$ is assumed to decay at $\tau\to\infty$ sufficiently fast that the integral in the right-hand side of Eq. (13) converges.

Substituting Eqs. (9) and (10) into Eq. (13) and using the periodic boundary condition, which can be rewritten in the form $A(\tau,\zeta+T)=A(\tau+T,\zeta)$, we obtain the transformation of the electric field envelope $A(\tau)\equiv A(\tau,\zeta_1)$ after a complete round trip in the cavity,

$$A(\tau+T) = \int_{-\infty}^{\tau} f(\tau-\theta)R(\theta)A(\theta)d\theta, \quad (14)$$

with

$$R(\tau) = \sqrt{\kappa}e^{(1-i\alpha_g)G(\tau)/2-(1-i\alpha_q)Q(\tau)/2}. \quad (15)$$

Here the attenuation factor $\kappa<1$ describes total nonresonant linear intensity losses per cavity round trip.

Equation (14) describes evolution of the electric field amplitude in a ring laser with arbitrary line shape of the spectral filtering element defined by the response function $f(\tau)$. In the case where spectral filtering element is absent, this function can be replaced by the Dirac delta function, $f(\tau)=\delta(\tau)$. Then Eq. (14) is transformed into the map

$$A(\tau+T) = R(\tau)A(\tau), \quad (16)$$

similar to the Ikeda map which was proposed to describe multistability and chaos in a ring cavity with nonlinear medium [15,16]. Equation (16) governs the time evolution of the amplitude A in a laser without spectral filtering element, i.e., in a situation considered by New [3]. An ML solution of these equations can be expressed as a T-periodic sequence of δ pulses, $|A(\tau)|^2=\Delta P\Sigma_{n=-\infty}^{\infty}\delta(\tau-nT)$, where ΔP is the dimensionless energy of a pulse. This solution is characterized by infinitely large number of locked modes which produce an infinitely short pulse.

Now let us consider the case where the response function in Eq. (14) is defined by

$$f(\tau) = \tilde{f}(\tau)H(\Delta-\tau), \quad \tilde{f}(\tau) = \frac{\gamma}{1-e^{-\gamma\Delta}}e^{(-\gamma+i\Omega)\tau}, \quad (17)$$

where $H(\tau)$ is the Heaviside step function and the parameter Ω describes detuning between the central frequency of the spectral filtering element and one of the cavity modes. In this case Eq. (14) can be replaced by the delay differential equation (DDE) with two delays:

$$\partial_\tau A(\tau) + (\gamma - i\Omega)A(\tau) = \tilde{f}(0)R(\tau-T)A(\tau-T) - \tilde{f}(\Delta)R(\tau-T_1)A(\tau-T_1). \quad (18)$$

Here $T_1=T+\Delta$. The solution of Eq. (18) can be written in the form

$$A(\tau+T) = e^{(-\gamma+i\Omega)\tau}C + \int_{\tau-\Delta}^{\tau} \tilde{f}(\tau-\theta)R(\theta)A(\theta)d\theta. \quad (19)$$

One can see that under the condition $C=0$ Eq. (19) is transformed into Eq. (14). This implies the following initial condition for the electric field amplitude:

$$A(0) = \sqrt{\kappa}\int_{-T_1}^{-T} \tilde{f}(-\tau)R(\tau)A(\tau)d\tau. \quad (20)$$

Equation (20) defines the initial condition for which Eq. (18) is equivalent to Eq. (14). However, since for $\gamma>0$ the term proportional to C in Eq. (19) decays exponentially with time, even for $C\neq 0$ the solution of Eq. (18) coincides with that of Eq. (14) in the limit $\tau\to\infty$. Therefore, for positive γ the precise form of the initial condition (20) can be safely dismissed in the calculations.

In order to clarify the physical meaning of Eqs. (17) let us consider two limiting situations. In the limit $\gamma\to 0$ we have $f(\tau)=\Delta^{-1}H(\Delta-\tau)\exp(-i\Omega\tau)$. The corresponding spectral filtering function is then defined by $\hat{f}(\omega)=\exp[-i(\omega-\Omega)\Delta/2]\sin[(\omega-\Omega)\Delta/2]/[\sqrt{2\pi}(\omega-\Omega)\Delta/2]^{-1}$, i.e., this case describes a reflection from a weak Bragg grating.

The second situation, $\Delta\to\infty$, corresponds to Lorentzian line shape of the bandwidth-limiting element, $f(\tau)=\gamma\exp[(-\gamma+i\Omega)\tau]$. In this case Eq. (14) can be replaced by differential equation with a single delay parameter equal to the cavity round-trip time T. After the coordinate change $A\to A\exp(i\Omega\tau)$ this equation takes the form

$$\gamma^{-1}\partial_\tau A(\tau) + A(\tau) = \sqrt{\kappa}e^{(1-i\alpha_g)G(\tau-T)/2-(1-i\alpha_q)Q(\tau-T)/2-i\varphi}A(\tau-T), \quad (21)$$

where $\varphi=\Omega T$.

The equations governing the evolution of the saturable gain and loss are obtained from Eqs. (11) and (12) by using Eqs. (9) and (10) to express $A(\tau,\zeta_2)$, $A(\tau,\zeta_3)$, and $A(\tau,\zeta_4)$ in terms of $A(\tau)=A(\tau,\zeta_1)$. They read

$$\partial_\tau G(\tau) = g_0 - \Gamma G(\tau) - e^{-Q(\tau)}(e^{G(\tau)}-1)|A(\tau)|^2, \quad (22)$$

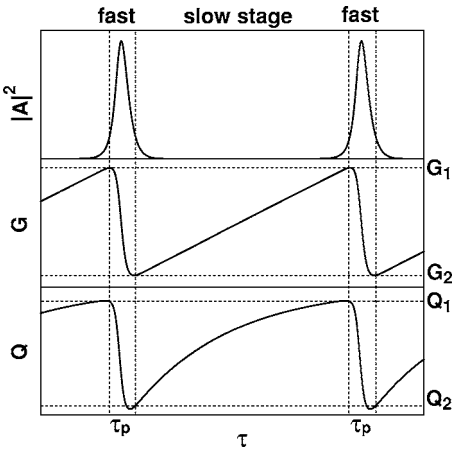

FIG. 2. Time evolution of the electric field intensity $|A|^2$, the saturable gain G, and the saturable loss Q in a mode-locked laser with slow absorber. Duration of the fast stage coincides with the pulse width τ_p. G_1 and Q_1 are the saturable gain and loss at the leading edge of a pulse which corresponds to the beginning of the fast stage and the end of the slow one. G_2 and Q_2 are the saturable gain and loss at the trailing edge of a pulse which corresponds to the end (beginning) of the fast (slow) stage.

$$\partial_\tau Q(\tau) = q_0 - Q(\tau) - s(1 - e^{-Q(\tau)})|A(\tau)|^2. \qquad (23)$$

In the following we will restrict our consideration to the analysis of Eqs. (21)–(23).

Note that an approach similar to that we have used to derive Eqs. (21)–(23) was applied earlier by Gurevich and Khanin to study passive ML in a solid-state laser [17–19]. However, the delay differential equations derived by these authors are singular at zero electric field. Therefore, our model is more suitable for analytical study in the limit of a slow saturable absorber in which the amplitude A becomes almost zero between ML pulses (see Sec. II A).

II. LIMIT OF INFINITELY BROAD BANDWIDTH

The number of cavity modes that take part in ML process can be roughly estimated as the ratio of the bandwidth of the spectral filtering element γ and the cavity intermode frequency spacing T^{-1}. In this section we perform analytical study of Eqs. (21)–(23) in the case where γT is large ($\gamma \to \infty$). In this limit the duration of a ML pulse $\tau_p \propto \gamma^{-1}$ vanishes, its amplitude $A_0 \propto \gamma^{1/2}$ diverges, while the pulse energy $\Delta P \propto A_0^2 \tau_p$ remains finite. Physically this means that the number of locked laser modes grows, while the energy associated with each separately taken mode decreases.

If γ is sufficiently large and the relaxation times of the intracavity media are large as compared with the pulse duration (slow absorber), then following the approach of New [3] and Haus [2], we split the evolution of a ML solution into two stages. At the slow stage, whose duration tends to the cavity round-trip time T as γ increases, the amplifying and absorbing media recover slowly between two subsequent pulses. During this stage the electric field intensity is close to zero, $|A(\tau)|^2 \approx 0$ (see Fig. 2). Therefore, the terms proportional to $|A(\tau)|^2$ in Eqs. (22) and (23) can be neglected at the slow stage. At the short fast stage the electric field intensity is large and therefore, the terms proportional to $|A(\tau)|^2$ dominate in Eqs. (22) and (23). The remaining (relaxation) terms in the right-hand sides of these equations can be neglected at the fast stage.

In this way, the laser equations can be solved separately for the slow stage and, under additional assumptions, for the fast stage. Then the full solution can be evaluated analytically by gluing the two ones. Below we demonstrate that both New and Haus classical approaches [2,3] can be recovered from our DDE model (21)–(23) under the approximation of small gain and loss per cavity round trip. Moreover, we generalize these results to the case where gain and loss per cavity round trip are not small, i.e., to a situation typical of semiconductor lasers. This will be done in Secs. II C and II D. As we will see, the generalized Haus approach is more precise, but has a smaller domain of applicability than the generalization of the New approach.

An important role in the analysis is played by the New's background stability criterion for ML pulses [3]. This criterion requires that the net gain $G(\tau) - Q(\tau) + \ln \kappa$ has to be negative during the entire slow stage. Physically this means that small perturbations of the low-intensity background between pulses decay with time (absolute stability). It can be shown that the background stability criterion is satisfied if the net gain is negative at the beginning and at the end of the slow stage. Therefore, it can be rewritten as a set of two inequalities

$$G_1 - Q_1 + \ln \kappa < 0, \quad G_2 - Q_2 + \ln \kappa < 0. \qquad (24)$$

Here G_2 and Q_2 (G_1 and Q_1) are the saturable gain $G(\tau)$ and loss $Q(\tau)$ evaluated at the beginning (end) of the slow stage (see Fig. 2). Since the end of the slow stage corresponds to the beginning of the fast one, and vice versa, the two inequalities in (24) give the background stability conditions at the leading and trailing edge of a pulse, respectively.

Obviously, the background stability criterion is of a qualitative nature. It does not take into account that the small perturbations can propagate along the low-intensity background until, after a finite time of order γ, they are absorbed by the leading or trailing edge of the pulse. This means that even when the background is unstable, the amplification of small perturbations does not necessarily destroy the ML pulse. The fact that stable ML pulses with unstable background can indeed exist is confirmed, e.g., by our numerics in Sec. III. It is natural to expect that such pulses should be more sensitive to noise than those with the stable background. We give a quantitative characterization of the sensitivity of the ML pulse to the background noise in Sec. IV.

A. Slow stage

Let us consider a solution of Eqs. (21)–(23) with periodic laser intensity corresponding to a ML regime (see Fig. 2). At the slow stage, when $|A(\tau)|^2 \approx 0$, Eqs. (22) and (23) become linear: $\partial_\tau G(\tau) = g_0 - \Gamma G(\tau)$, $\partial_\tau Q(\tau) = q_0 - Q(\tau)$. Solving these equations, we express the saturable gain G_1 and loss Q_1 at the leading edge of a pulse via their values G_2 and Q_2 at the trailing edge:

$$G_1 = G_2 e^{-\Gamma T} + \frac{g_0}{\Gamma}(1 - e^{-\Gamma T}), \tag{25}$$

$$Q_1 = Q_2 e^{-T} + q_0(1 - e^{-T}). \tag{26}$$

Here T is the duration of the slow stage that is equal to the cavity round-trip time in the limit $\gamma \to \infty$.

Eqs. (25) and (26) can be further simplified in the two limiting cases.

(i) The absorber relaxes completely between two subsequent pulses, i.e., $T \ll 1$. Then, instead of Eq. (26) we obtain

$$Q_1 = q_0. \tag{27}$$

(ii) The relaxation time of the gain medium is much smaller than the cavity round-trip time, i.e., $\Gamma T \ll 1$. In this case Eq. (25) can be replaced by $G_1 = G_2 + g_0 T$.

B. Fast stage

At the fast stage we neglect the relaxation terms in the right-hand sides of Eqs. (22) and (23). Then, introducing the dimensionless differential pulse energy $P(\tau) = \int_0^\tau |A(\theta)|^2 d\theta$, where $\tau = 0$ corresponds to the beginning of the fast stage, we rewrite these two equations in the form

$$\partial_P g(P) = -e^{-q(P)}(e^{g(P)} - 1), \quad \partial_P q(P) = -s(1 - e^{-q(P)}), \tag{28}$$

with $g(P) = G(\tau)$ and $q(P) = Q(\tau)$. Solving Eqs. (28) we express the saturable gain $G_2 = g(\Delta P)$ and loss $Q_2 = q(\Delta P)$ at the trailing edge of a pulse via their values $G_1 = g(0)$ and $Q_1 = q(0)$ at the leading edge

$$G_2 = g(\Delta P) = -\ln\left(1 - \frac{1 - e^{-G_1}}{[e^{-Q_1}(e^{s\Delta P} - 1) + 1]^{1/s}}\right), \tag{29}$$

$$Q_2 = q(\Delta P) = \ln[1 + e^{-s\Delta P}(e^{Q_1} - 1)]. \tag{30}$$

Here $\Delta P = P(\tau_p) = \int_0^{\tau_p} |A(\tau)|^2 d\tau$ is the total dimensionless energy of a ML pulse.

By taking modulus square from both sides of Eq. (21), and integrating over the pulse duration τ_p we obtain

$$\gamma^{-2} \int_0^{\tau_p} |\partial_\tau A(\tau)|^2 d\tau + \Delta P = \kappa \int_0^{\tau_p} e^{G(\tau) - Q(\tau)} |A(\tau)|^2 d\tau. \tag{31}$$

Then, using the solutions of Eqs. (28), the integral in the right-hand side can be calculated explicitly. This yields the relation

$$\gamma^{-2} \int_0^{\tau_p} |\partial_\tau A(\tau)|^2 d\tau + \Delta P = \kappa \ln \frac{e^{G_1} - 1}{e^{G_2} - 1}. \tag{32}$$

Note that the integral term in the left-hand side, which describes energy losses introduced by the spectral filtering element, remains finite at $\gamma \to \infty$, i.e., strictly speaking, it cannot be neglected even in the limit of infinitely broad bandwidth. Indeed, as was pointed out by Haus [2], it is obvious that $|\partial_\tau A(\tau)|^2 \propto \gamma^2 |A(\tau)|^2$ for pulses of width $\tau_p \propto \gamma^{-1}$. In other words, the spectral width of the ML pulse increases with the bandwidth of the spectral filtering element in such a way that the losses introduced by this element remain finite in the limit $\gamma \to \infty$.

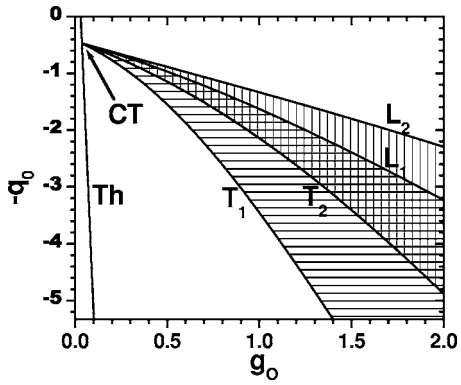

FIG. 3. Background stability domains calculated using the generalization of New's approach described in Sec. II C. The horizontally (vertically) hatched area presents the background stability domain for a fundamental ML regime (a regime with twice higher repetition rate). Straight line Th corresponds to the linear threshold. The curves $L_{1,2}$ and $T_{1,2}$ indicate the leading and trailing edge instability boundaries, respectively. CT is the codimension-2 point defined by Eqs. (34). The parameters are $T = 1.875$, $s = 25$, $\Gamma = 1.33 \times 10^{-2}$, $\kappa = 0.1$.

Thus, in order to get an analytical description of the fast stage one has to express the integral in the left hand side of Eq. (32) explicitly in terms of the pulse parameters. Two particular situations when this can be done analytically are studied in the following Secs. II C and II D.

C. A generalization of New's model

New's approach assumes the absence of spectral filtering in the cavity. In this case $f(\tau) = \delta(\tau)$ in Eq. (14) and, therefore, such approximation is equivalent to the neglect of the derivative term $\gamma^{-1}\partial_\tau A(\tau)$ in Eq. (21). This means dropping the integral term in the left-hand side of Eq. (32), i.e., the equation becomes

$$\Delta P = \kappa \ln \frac{e^{G_1} - 1}{e^{G_2} - 1}. \tag{33}$$

Equations (25), (26), (29), and (30), along with Eq. (33), constitute a closed set of equations that can be solved for $G_{1,2}$, $Q_{1,2}$, and ΔP. This gives the dependence of the pulse energy ΔP on the laser parameters. As we have already mentioned, the neglect in Eq. (32) of the term describing the losses introduced by spectral filtering cannot be justified even for infinitely large γ. Therefore, relation (32) is only a crude approximation. Still, as we will see, it can be satisfactory for a large domain of parameters.

Substituting the solution into inequalities (24) one can calculate the background stability boundaries of a ML pulse. A result of such calculation is presented in Fig. 3 for ML solutions with the period T and $T/2$. The first of them corresponds to a fundamental ML regime with a single pulse circulating in the cavity, while the second one corresponds to a

regime with twice greater repetition rate and two pulses in the cavity. One can see that the two stability domains overlap in certain parameter range. This indicates the possibility of a hysteresis between the regimes having different repetition rates. According to Fig. 3, the two background stability boundaries, namely, those for the leading and trailing edges of a pulse, meet at the codimension-2 point CT lying on the linear threshold line Th. This point can be calculated explicitly:

$$q_0 = \ln \frac{\kappa(s-1)}{s\kappa - 1}, \quad g_0 = \Gamma \ln \frac{s-1}{s\kappa - 1}. \tag{34}$$

It is well known [7] that ML pulses with stable background can exist only if the absorbing medium is saturated faster than the gain one [2], i.e., when $s>1$. It follows from Eqs. (34) that in a situation when gain and loss per cavity round trip are not small, such pulses are possible only if the more strict condition

$$s\kappa > 1 \tag{35}$$

is satisfied. In the small-gain and -loss limit ($\kappa \to 1$) this new condition coincides with the condition $s>1$. However, for the parameter values typical of semiconductor lasers with their high losses ($\kappa \ll 1$) the inequality (35) implies much stronger limitation on the minimal value of the ratio of saturation intensities than the previously known condition $s>1$. For $s\kappa>1$ the parameter range of ML pulses with stable background enlarges with the product $s\kappa$. This is in qualitative agreement with the experimental results of Ref. [20] where it was shown that the quality of a ML regime can be improved by decreasing the nonresonant losses.

Equations (25), (26), (29), (30), and (33) can be considered as a generalized New's model because unlike the equations for the pulse parameters derived in Ref. [3] they do not assume that gain and loss per cavity round trip are small. In order to recover from these equations those obtained by New we expand Eqs. (29) and (30) up to the first-order terms in G_1 and Q_1:

$$G_2 = G_1 e^{-\Delta P}, \quad Q_2 = Q_1 e^{-s\Delta P}. \tag{36}$$

Then, substituting Eq. (29) into Eq. (33) and expanding it up to the first-order terms in G_1, Q_1, and $\ln \kappa$ we obtain the equation for the pulse energy

$$G_1(1-e^{\Delta P}) - Q_1 \frac{(1-e^{s\Delta P})}{s} - \Delta P \ln \kappa = 0, \tag{37}$$

which is equivalent to Eqs. (11) and (12) of Ref. [3].

Background stability boundaries of ML pulses calculated using different sets of equations are presented in Fig. 4. In this figure dashed lines L_N and T_N indicate the leading and trailing edge instability boundaries obtained with the pulse parameters calculated using Eqs. (25), (27), (36), and (37). These equations are equivalent to those derived by New [3]. Solid lines L_N and T_N indicate background instability boundaries calculated using the generalization of New's model described in this section. Dots in Fig. 4 represent points at the background stability boundaries which have been calculated by means of direct numerical integration of Eqs. (21)–(23)

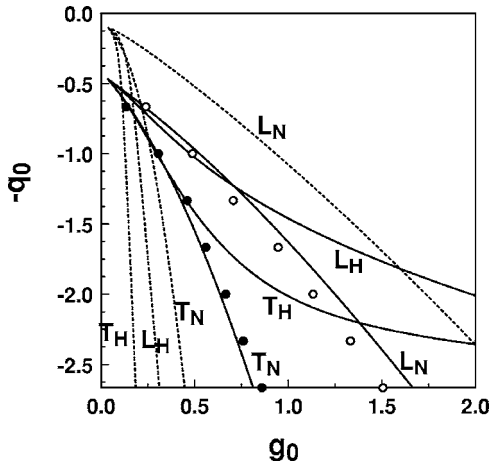

FIG. 4. Background stability boundaries calculated using four different sets of equations. Solid lines L_N and T_N indicate the leading and trailing edge instability boundaries obtained using the generalized New model. Solid lines L_H and T_H indicate similar boundaries obtained using the generalized Haus model. The corresponding instability boundaries calculated using the original New and Haus equations are shown by dashed lines. Filled (empty) dots indicate trailing (leading) edge instability boundary calculated by numerical integration of Eqs. (21)–(23). Parameters are the same as in Fig. 3 (with $\alpha_g=\alpha_q=\varphi=0$).

with $\gamma=333$. It is noteworthy that with the decrease of γ the width of the background stability domain increases. One can see from Fig. 4 that, despite neglecting the losses introduced by spectral filtering, the generalized New model appears to be in a quite good agreement with the results of numerical integration of the DDE model. On the other hand, discrepancy between the numerical data and the results obtained using the original New equations [3] is significant. This is because Fig. 4 corresponds to parameter values typical of semiconductor lasers characterized by large gain and loss per cavity round trip.

Note that within the framework of New's approach, in which the derivative term is neglected in Eq. (21), the background stability boundaries do not depend on the linewidth enhancement factors $\alpha_{g,q}$. This is not true any longer as soon as spectral filtering is taken into account.

D. A generalization of Haus's model

In this section we study a situation when the gain and absorbing media are weakly saturated by ML pulses. In this case one can obtain an explicit expression for the pulse shape by solving analytically the fast-stage equations. Let us consider the ML solution $A(\tau+T)=e^{i\psi}A(\tau-\delta T)$ with periodic laser intensity. Here $\delta T=T_p-T$ is the small difference between the pulse repetition period T_p and the cavity round-trip time. Substituting this solution into Eq. (21) we get

$$\gamma^{-1}\partial_\tau A(\tau-\delta T) + A(\tau-\delta T) = \sqrt{\kappa} e^{(1-i\alpha_g)g(P)/2-(1-i\alpha_q)q(P)/2-i(\varphi+\psi)} A(\tau). \tag{38}$$

In Eq. (38) $g(P)$ and $q(P)$ are the solutions of the fast stage equations (28). In the limit $\gamma \to \infty$ corresponding to infinite

bandwidth of the spectral filtering element the duration of the pulse vanishes and the period of ML solution tends to the cavity round-trip time, i.e., $\tau_p, \delta T \propto \gamma^{-1}$. Introducing in this limit the rescaled time variable $\zeta=\gamma\tau$ we rewrite Eq. (38) in the form

$$\partial_\zeta a(\zeta-c)+a(\zeta-c)=F(P)a(\zeta), \tag{39}$$

where $a(\zeta)=\gamma^{-1/2}A(\tau)$, $P(\zeta)=\int_{-\infty}^{\zeta}|a(s)|^2ds$, and $c=\lim_{\gamma\to\infty}(\gamma\delta T)$. The function $F(P)$ is obtained by substituting the solutions of Eqs. (28) into Eq. (38):

$$F(P)=\sqrt{\kappa}e^{-i(\varphi+\psi)}\left[\left[1+e^{-sP(\zeta)}(e^{Q_1}-1)\right]^{(1-i\alpha_q)}\times\left(1-\frac{1-e^{-G_1}}{(e^{sP(\zeta)-Q_1}-e^{-Q_1}+1)^{1/s}}\right)^{(1-i\alpha_g)}\right]^{-1/2}. \tag{40}$$

Equations (39) and (40) describe a ML pulse shape in the limit of infinitely broad Lorentzian bandwidth. For a laser operating close enough to the threshold, the normalized pulse energy is small $P(\zeta)\leqslant\Delta P\ll 1/s$, which means that both the absorber and the amplifier are weakly saturated. Under this approximation, which underlies Haus's theory [2], Eqs. (29) and (30) together with the function $F(P)$ in Eq. (39) can be expanded in power series up to the second-order terms in $P(\zeta)$. Substituting this expansion into Eq. (39) we obtain

$$c\left(\frac{c}{2}-1\right)\partial_{\zeta\zeta}a(\zeta)-(1-c)\partial_\zeta a(\zeta)+\left(F_0-1+F_0'P(\zeta)+\frac{F_0''}{2}P(\zeta)^2\right)a(\zeta)=0. \tag{41}$$

where F_0, F_0', and F_0'' denote the function $F(P)$ and its derivatives all evaluated at $P=0$. In Eq. (41) we have used the approximation $a(\zeta-c)\approx a(\zeta)-ca_\zeta(\zeta)+c^2\partial_{\zeta\zeta}a(\zeta)/2$ which implies parabolic gain dispersion. This approximation assuming that the third- and higher-order derivatives of $a(\zeta)$ are much smaller than the second derivative is valid for a laser operating near the lasing threshold. A solution of Eq. (41) can be written in the form [7,21]

$$a(\zeta)=\sqrt{\frac{\Delta P}{2\zeta_p}}e^{i\Omega\zeta}\mathrm{sech}^{(1+i\beta)}\left(\frac{\zeta}{\zeta_p}\right), \tag{42}$$

where ΔP is the dimensionless pulse energy, $\zeta_p=\gamma\tau_p$ is the normalized pulse width, and β and Ω describe, respectively, the chirp and normalized frequency shift of the ML solution. Substituting Eq. (42) into Eq. (41) and equating coefficients in front of different powers of the hyperbolic tangent, we obtain six real equations for six unknown parameters: ΔP, ζ_p, β, Ω, c, and ψ. In the particular case when $\alpha_g=\alpha_q=\varphi=0$ we have $\beta=\Omega=\psi=0$. In this case elimination of ζ_p and c leads to the following quadratic equation for the pulse energy:

$$2(F_0-1)+F_0'\Delta P+\frac{3F_0''}{8}\Delta P^2=0, \tag{43}$$

with real F_0, F_0', and F_0''.

Solving Eqs. (43), (25), (26), (29), and (30) for the pulse parameters $G_{1,2}$, $Q_{1,2}$, and ΔP and substituting the solutions into the inequalities (24), we get the background stability boundaries for the sech solution defined by Eq. (42). This generalizes analytical results obtained by Haus [2] to the case of large gain and losses.

One can easily check using Eq. (40) that the equation $F_0=1$, corresponds to zero net gain at the beginning of the fast stage. Hence, this equation defines the leading edge background instability boundary. Furthermore, according to Eq. (43), the two conditions $F_0=1$ and $F_0'=0$ define a codimension-2 point where the leading edge instability boundary hits the lasing threshold. Solving these equations for G_1 and Q_1 and taking into account that at $\Delta P=0$ one has $G_1=G_2=g_0/\Gamma$ and $Q_1=Q_2=q_0$ we recover the codimension two point (34). Hence, the background stability boundaries calculated using the generalizations of New's and Haus's approaches originate from the same point in the parameter space.

In the limit of small gain and loss per cavity round trip the generalized model derived in this section is reduced to the original Haus equations. To demonstrate this, we expand Eq. (43) into power series up to the first-order terms in G_1, Q_1, and $\ln\kappa$. Then we obtain the following equation for the normalized pulse energy:

$$G_1-Q_1+\ln\kappa-\frac{1}{2}(G_1-sQ_1)\Delta P+\frac{3}{16}(G_1-s^2Q_1)\Delta P^2=0. \tag{44}$$

In the limit when $G_1\ll s^2Q_1$ it is equivalent to Eq. (36) of Ref. [2].

In Fig. 4 leading and trailing edge instability boundaries calculated using the original Haus equations [2] are shown by dashed lines L_H and T_H, respectively. The same boundaries obtained using the generalization of the Haus model described in this section are indicated by solid lines L_H and T_H. One can see that similarly to the original New model the original Haus model is not capable of describing ML in parameter domain of semiconductor lasers. According to Fig. 4, the generalized Haus' equations work well only when the pulse energy is small enough. The discrepancy between the instability boundaries calculated using these equations and those obtained by direct numerical integration of Eqs. (21)–(23) increases with the pulse energy. On the other hand, the results obtained using the generalized New approach remain in quite good agreement with the results of numerical simulations even for strong saturation.

III. NUMERICAL RESULTS

As we have shown in the preceding sections, the delay differential formulation of the ML problem allows for performing analytical study in the limit $\gamma\to\infty$. Another important advantage of this formulation is that it permits one to make use of numerical techniques that have been developed for the analysis of delay differential equations. In particular, Eqs. (21)–(23) can be easily simulated and their bifurcations can be traced in the parameter space with the help of stan-

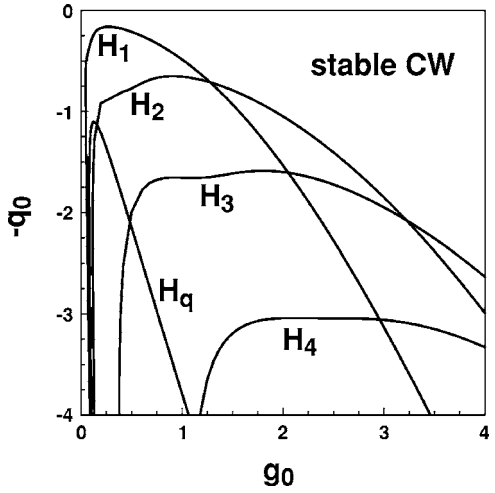

FIG. 5. Andronov-Hopf bifurcations of the cw solution of Eqs. (21)–(23). Curves H_n indicate Andronov-Hopf bifurcations with the frequency $\Omega_n \approx 2\pi n/T (n=1,2,3,4)$. Curve H_q corresponds to the Andronov-Hopf bifurcation with Q-switching frequency. $\gamma=33.3$, $\alpha_{g,q}=0$, $\varphi=0$. Other parameters are the same as in Fig. 3.

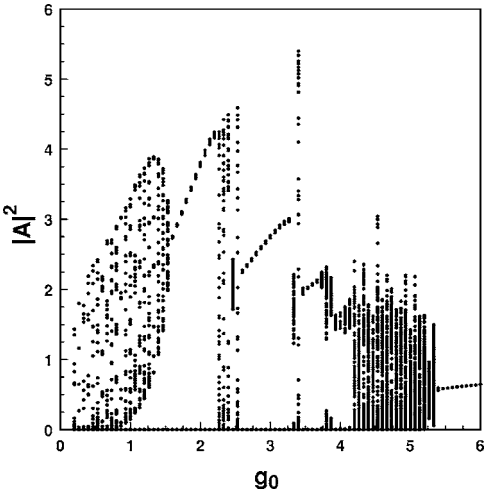

FIG. 6. Bifurcation diagram obtained by direct numerical simulation of Eqs. (21)–(23) with $q_0=4.0$. Other parameters are the same as in Fig. 5.

dard numerical codes. In this section we present the results of numerical analysis of Eqs. (21)–(23) with $T=1.875$, $\kappa=0.1$, $\Gamma=1.33\times10^{-2}$, and $\varphi=0$. The simplest stationary solution of Eqs. (21)–(23) corresponds to zero electric field intensity (laser off):

$$A=0, \quad G=g_0/\Gamma, \quad Q=q_0. \tag{45}$$

Apart from this trivial steady state, Eqs. (21)–(23) can exhibit continuous wave (cw) solutions in the form $A(\tau)=A_0 e^{i\gamma\omega\tau}$. The normalized time-independent intensity of the cw solution and its normalized frequency shift ω can be found by solving the equations

$$\kappa e^{G-Q} - 1 - \omega^2 = 0, \tag{46}$$

$$\omega + \tan[\gamma T\omega + (\alpha_g G - \alpha_q Q)/2 - \phi] = 0, \tag{47}$$

where G and Q are expressed in terms of the laser intensity $|A_0|^2$ by equating to zero the right-hand sides of Eqs. (22) and (23); the condition $\cos[\gamma T\Omega + (\alpha_g G - \alpha_q Q)/2 - \phi] > 0$ must be satisfied in addition to relations (46) and (47). Transcendental equations (46) and (47) have multiple solutions, each corresponding to a certain cavity mode. The frequency spacing between two adjacent cw solutions coincides with the cold-cavity intermode frequency spacing in the limit $\gamma \to \infty$. Let the cw solution with $\omega=\omega_0$ have the smallest absolute value of frequency detuning $|\omega_0|$. This solution characterized by the smallest effective losses bifurcates from the steady state (45) at the linear threshold point $g_0=\Gamma[q_0 - \ln\kappa + \ln(1+\omega_0^2)]$. All the other cw solutions have greater threshold currents and therefore they bifurcate from the trivial steady state when it is already unstable. In Fig. 5 we summarize the results of the linear stability analysis of the cw solution with $\omega=\omega_0$, which has been performed with the help of the DDEBIFTOOL package [22]. In this figure Andronov-Hopf bifurcation curve H_1 gives rise to a periodic solution that, when stable, corresponds to a fundamental ML regime with the pulse repetition period close to the cavity round-trip time T. The Andronov-Hopf bifurcation curves H_n with $n=2,3,4$ signal the onset of (yet typically unstable) multiple pulse ML regimes with the repetition periods $T_n \approx T/n$. The curve H_q indicates the Andronov-Hopf bifurcation with the period approximately one order of magnitude greater than T for the parameter values of Fig. 5. This frequency is associated with the Q-switching instability.

The results of direct numerical integration of the DDE model by means of the RADAR5 package [23] are presented in Figs. 6–10. Bifurcation diagram in Fig. 6 shows extrema of the laser intensity time dependence calculated for different values of the pump parameter g_0. To calculate this diagram we have used the following procedure. First, Eqs. (21)–(23) have been integrated from $\tau=0$ to $\tau \approx 2\times10^3$ in order to skip transient behavior. Next, during the time interval $\Delta\tau \approx 200$, the maxima and minima of the intensity time trace have been plotted for each given value of g_0. As we see in Fig. 6, when the pump parameter g_0 is small enough, the laser exhibits a regime with pulse power modulated in time by the Q-switching frequency. The intensity time trace illustrating this regime is shown in Fig. 7(a). With the further increase of

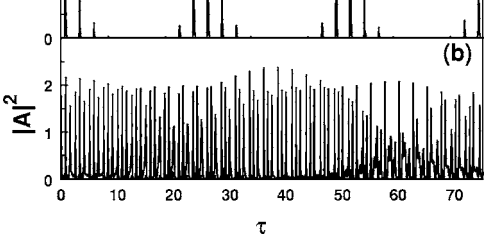

FIG. 7. Nonperiodic intensity time traces. (a) ML solution modulated by Q-switching frequency $g_0=0.67$; (b) a regime that appears after the breakup of the periodic ML regime shown in Fig. 8(c), $g_0=4.67$. The other parameters are the same as in Fig. 6.

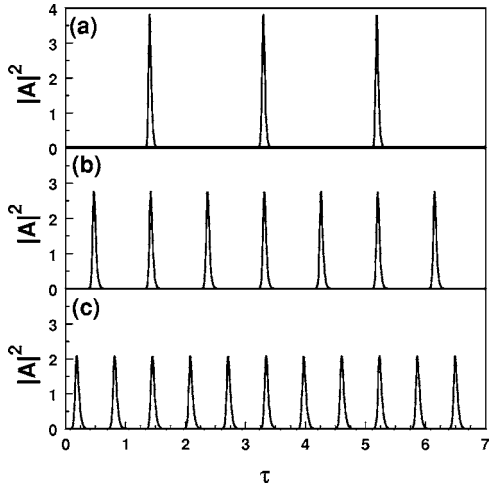

FIG. 8. Periodic intensity time traces corresponding to different ML regimes. (a) Fundamental ML regime, $g_0=2.0$; (b) ML regime with two pulses in the cavity, $g_0=3.0$; (c) ML regime with three pulses in the cavity, $g_0=3.6$.

g_0, the modulation regime undergoes a backward Andronov-Hopf bifurcation and a transition to a fundamental periodic ML regime [shown in Fig. 8(a)] occurs; note that an analytical study of Q-switching bifurcation of the ML regime was performed in Ref. [24] within the framework of the Haus master equation. With the further increase of the pump parameter a transition to regimes with approximately two and three times higher pulse repetition frequency happens [see Figs. 8(b) and 8(c)]. These regimes are characterized by a pulse peak intensity smaller than that of the fundamental ML regime. The breakup of ML behavior occurs with the sudden onset of chaotic modulation of the pulse power [see the intensity time trace shown in Fig. 7(b)]. Finally, at large gains the laser undergoes a transition to cw operation with the

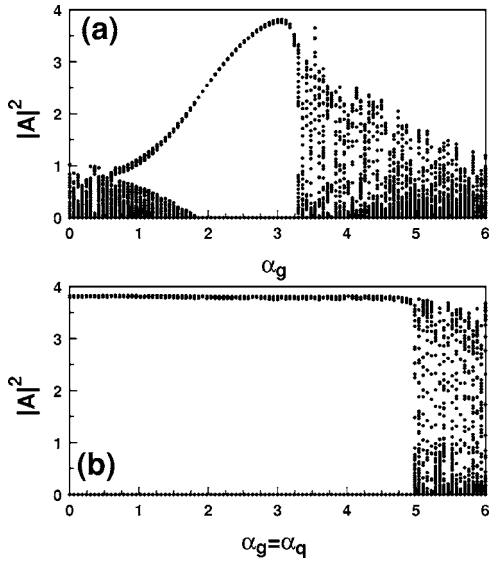

FIG. 9. Bifurcation diagrams obtained by changing the linewidth enhancement factors, $g_0=2.0$. (a) Extrema of the intensity time trace vs $\alpha_g, \alpha_q=3.0$. (b) Extrema of the intensity time trace vs $\alpha_g=\alpha_q$. The other parameters are the same as in Fig. 6.

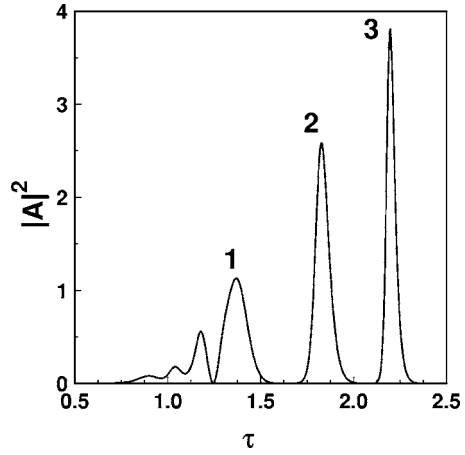

FIG. 10. ML pulse shape. (1) $\alpha_g=1.0$; (2) $\alpha_g=2.0$; (3) $\alpha_g=3.0$. Other parameters are the same as in Fig. 9.

electric field intensity independent of time. The bifurcation diagram in Fig. 6 appears to be in a qualitative agreement with the experimental results of Refs. [20,25] where a gradual transition from a self-pulsing regime to a ML one was observed with the increase of the injection current in the gain section. An experimental observation of a regime with repetition period equal approximately to one-half of the cavity round-trip time in a passively mode-locked ring semiconductor laser was reported in Ref. [26].

Figure 9 has been obtained in a similar way as Fig. 6, with the linewidth enhancement factors taken as bifurcation parameters instead of g_0. According to Fig. 9(a) which corresponds to $\alpha_q=3.0$, the shortest ML pulses with the largest peak power are observed in the situation when the linewidth enhancement factors in the two sections are equal, $\alpha_g=\alpha_q$. Such pulses are also characterized by the shortest width, as is illustrated by Fig. 10. With the decrease of the linewidth enhancement factor in the gain section ($\alpha_g<\alpha_q$) the ML pulse broadens, its amplitude decreases and finally a transition to a regime with nearly quasiperiodic laser intensity takes place. This regime is characterized by sharp intensity oscillations at the leading edge of ML pulse (curve 1 in Fig. 10). The effect of the increase of α_g above α_q is even more pronounced: very soon a transition from the ML regime with periodic laser intensity to a chaotic regime takes place. We have found that this transition is associated with the intermittency between ML solution and chaotic intensity pulsations. Indeed, slightly above the transition point, time intervals characterized by almost regular ML behavior alternate with irregular spiking. The duration of these "regular" time intervals decreases with the increase of α_g, and finally a fully chaotic regime develops. The fact that the best quality of ML pulses has been observed at $\alpha_g=\alpha_q$ can be intuitively explained by the fact that gain and loss enter Eq. (21) with opposite signs. Therefore, contributions of the linewidth enhancement factors must compensate each other, at least partially, when $\alpha_g\alpha_q>0$. According to our numerical results, the most complete compensation takes place for $\alpha_g=\alpha_q$, i.e., when the frequencies ω of the cw solutions are independent of the linear gain and loss parameters. In the case when the linewidth enhancement factors in the two sections are equal,

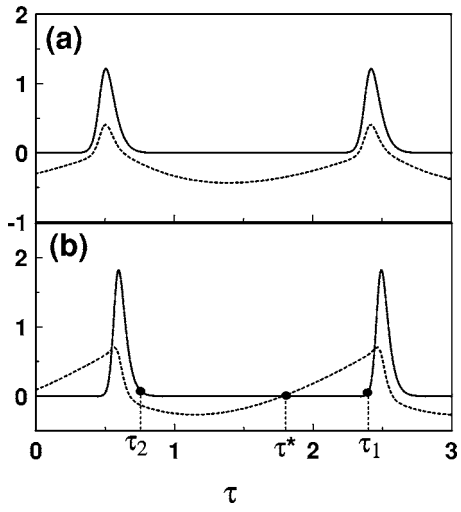

FIG. 11. Time dependencies of the laser intensity (solid line) and the net gain parameter (dashed line). $\alpha_g=\alpha_q=2.0$, $q_0=2.67$, $\gamma=15$. (a) ML pulses with stable background, $g_0=1.2$; (b) ML pulses with unstable background at the leading edge, $g_0=1.67$. Other parameters are the same as in Fig. 5.

their increase almost does not affect the pulse peak power, as can be seen from Fig. 9(b). The breakup of the ML regime (at $\alpha_g=\alpha_q>5$) leads to a sudden development of a chaotic behavior.

Figure 11 shows the time dependencies of the electric field intensity and the round-trip net gain parameter $\mathcal{G}(\tau)=G(\tau)-Q(\tau)+\ln\kappa$ for two fundamental ML regimes corresponding to different pump parameters. In Fig. 11(a) corresponding to $g_0=1.2$ the net gain is negative between pulses and becomes positive only during short time intervals when the pulse amplitude is large. Therefore, the solution shown in this figure has a stable background according to New's criterion. On the contrary, Fig. 11(b) corresponding to $g_0=1.67$ presents a stable periodic solution of Eqs. (21)–(23) having an unstable background at the leading edge. The existence of stable ML pulses with unstable background at the trailing edge in passively mode-locked laser was theoretically predicted in Refs. [9,27]. Pulses with unstable background at the leading edge similar to those shown in Fig. 11(b), were found up to now only in models of synchronously pumped mode-locked lasers [28–30]. Note that the physical mechanisms of the unstable background formation are different in actively and passively mode-locked lasers. In Fig. 11(b) the net gain window is opened in the course of the carrier density relaxation process: For the parameter values typical of semiconductor lasers, gain recovers very slowly ($\Gamma\ll 1$), and continues to recover when the absorption has already almost completely achieved its unsaturated value. As a result, a net gain window appears. It is caused neither by the arrival of a pulse, as in the classical passive ML mechanism [3], nor by external pumping, as in the active ML. As we have already mentioned, the background instability does not automatically cause the instability of the ML regime as a whole. We analyze the effect of background perturbations in the next section.

IV. EFFECT OF SPONTANEOUS EMISSION NOISE

In this section we take into account the spontaneous emission noise by adding a noise source of a certain power D in the right-hand side of Eq. (21). Since the main effect of the perturbations consists in filling the low-intensity intervals between pulses with stochastic background [28], we consider Eq. (21) at the slow stage of the ML solution where the saturable gain $G(\tau)$ and loss $Q(\tau)$ obey Eqs. (25) and (26). At the slow stage, when γ is large, one may use the approximation $A(\tau+\gamma^{-1})\sim\gamma^{-1}\partial_\tau A(\tau)+A(\tau)$ in the left-hand side of Eq. (21), which transforms this equation into the map

$$A(\tau+T+\gamma^{-1})=R(\tau)A(\tau)+B(\tau), \tag{48}$$

where $B(\tau)$ describes the noise, and $R(\tau)$ is defined by Eq. (15). Note that Eq. (48) does not take into account spectral filtering any longer. In order to include this filtering into consideration, we assume that the time evolution of the noise term in Eq. (48) is described by the Ornstein-Uhlenbeck process

$$\gamma^{-1}\partial_\tau B(\tau)+B(\tau)=\sqrt{D}\chi(\tau),$$

where $\chi(\tau)$ is the δ-correlated noise source, $\langle\chi(\tau)\chi^*(\tau')\rangle=\delta(\tau-\tau')$. The dispersion of $B(\tau)$ is then given by $\frac{1}{2}\gamma D(1-e^{-\gamma\tau})$.

Since the period of the ML pulse behaves as $T_p\sim T+c\gamma^{-1}$, we see from Eq. (48) that after each round trip the perturbations caused by the noise propagate toward the leading edge of a pulse when $c<1$ and toward the trailing edge when $c>1$. The corresponding velocity per round trip is given by $v=(1-c)/\gamma$. Depending on the sign of the net gain parameter, the perturbations can decay or grow in the course of propagation. It follows from Eq. (48) that after k round trips the amplitude of the background perturbation is

$$A_k(\tau)=\sum_{m=1}^{k}B[\tau-m(T_p+v)]\prod_{j=1}^{m-1}e^{ij\psi}R(\tau-jv),$$

where we have used the property that for the ML solution $R(\tau)$ is periodic up to the phase shift ψ, i.e., $R(\tau+T_p)=R(\tau)e^{i\psi}$. The averaged power can be estimated as

$$P_k(\tau)=\langle A_k(\tau)A_k^*(\tau)\rangle\sim\frac{\gamma}{2}D\sum_{m=1}^{k}\exp\left(\sum_{j=1}^{m-1}\mathcal{G}(\tau-jv)\right), \tag{49}$$

where $\mathcal{G}(\tau)=G(\tau)-Q(\tau)+\ln\kappa$ is the net gain parameter. Below we restrict our consideration to the case where the perturbations are delayed with respect to the pulses, i.e., $v>0$. In all our simulations, e.g., for the parameter values of Fig. 11(b), the stable ML pulses with unstable background at the leading edge always satisfied this condition. The pulses with $v<0$ and with unstable background at the trailing edge can be considered in a similar way.

Since the velocity $v\propto\gamma^{-1}$ is small, using the trapezoidal rule we can estimate the sum in the exponent in Eq. (49) as

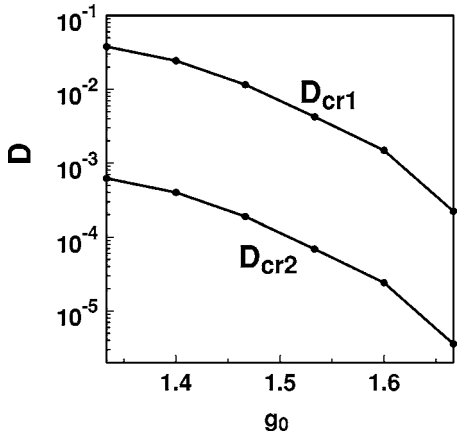

FIG. 12. Dependence of the critical noise powers given by Eqs. (52) and (53) on the linear gain parameter. The other parameters are the same as for Fig. 11(b).

$$\sum_{j=1}^{m-1} \mathcal{G}(\tau - jv) = v^{-1} \int_{\tau-(m-1/2)v}^{\tau-v/2} \mathcal{G}(\theta) d\theta + O(v).$$

Then the power of the background fluctuations is estimated as

$$P(\tau) = DS(\tau)$$

$$\text{with } S(\tau) \sim \frac{\gamma}{2} \sum_{m \geqslant 1, \sigma_m \geqslant \tau_2} \exp\left(v^{-1} \int_{\sigma_m}^{\tau-v/2} \mathcal{G}(\theta) d\theta \right),$$

where $\sigma_m \equiv \tau - (m-1/2)v$ and $\tau = \tau_2$ corresponds to the beginning of the slow stage [see Fig. 11(b)]. Since v^{-1} is large, the main contribution to the sum is given by the values of σ close to those corresponding to the maxima of the cumulative gain $\int_{\sigma}^{\tau-v/2} \mathcal{G}(\theta) d\theta$. This allows us to obtain the estimates

$$S(\tau) \sim \frac{\gamma}{2} [1 - \exp \mathcal{G}(\tau)]^{-1}, \tag{50}$$

$$S(\tau) \sim \gamma \sqrt{\frac{\pi}{2v\mathcal{G}'(\tau^*)}} \exp\left(v^{-1} \int_{\tau^*}^{\tau} \mathcal{G}(\theta) d\theta - \frac{1}{2} \mathcal{G}(\tau) \right), \tag{51}$$

where (50) corresponds to the net gain $\mathcal{G}(\theta)$ negative for all $\tau_2 \leqslant \theta \leqslant \tau$, and (51) corresponds to the net gain changing its sign from negative to positive at $\theta = \tau^*$ near the leading edge of the next pulse [see Fig. 11(b)]. At τ close to τ^* one has to use an appropriate matching between (50) and (51) (we omit the formulas).

In the case of unstable background at the leading edge, the power of the background fluctuations grows with τ, i.e., $S(\tau)$ attains its maximum $\mathcal{S} = S(\tau_1)$ at the end of the slow stage. For computational purposes we define τ_1 as the moment when the nonlinear term in Eq. (23) becomes equal to the relaxation term, i.e., $\partial_\tau Q(\tau_1) = 0$. Since the gain section recovers and saturates much more slowly than the absorber one, the similar event $\partial_\tau G = 0$ in Eq. (22) happens usually at larger τ.

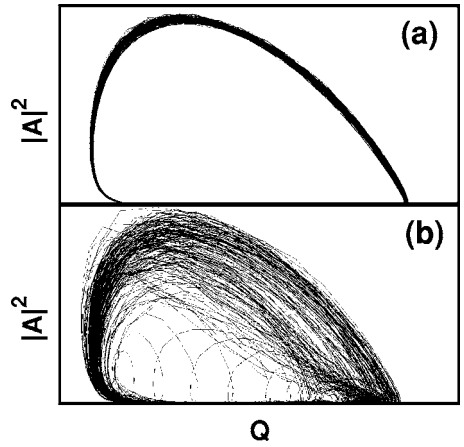

FIG. 13. Phase portraits of noisy ML solutions. $g_0 = 1.6$. (a) $D \approx D_{cr2}$. (b) $D \approx D_{cr1}$. Parameters are the same as for Fig. 11(b).

We can now define the critical level of noise, above which the ML solution can be destroyed, as

$$D_{cr1} \sim \mathcal{S}^{-1}. \tag{52}$$

For smaller D the ML pulse can be preserved, but still the effect of noise on the pulse shape and on the duration of the interval between pulses can be quite profound. To measure this effect, we compare the power of background fluctuations with the power of electromagnetic field for the unperturbed ML pulse at the beginning of the fast stage $\tau = \tau_1$. The latter power is obtained by equating the right hand side of Eq. (23) to zero, i.e., $|A|^2 = s^{-1}(q_0 - Q)/(1 - e^{-Q})$. Thus, we find the second critical value of the noise power, above which the effect of noise on the ML pulse shape can become significant:

$$D_{cr2} \sim (q_0 - \mathcal{Q})/[s(1 - e^{-\mathcal{Q}})\mathcal{S}], \tag{53}$$

where $\mathcal{Q} = Q(\tau_1)$ and $\mathcal{S}$ are evaluated at the end of the slow stage.

In Fig. 12 the dependence of the two critical values of the noise power [see Eqs. (52) and (53)] on the linear gain parameter g_0 is shown for the pulses having unstable background at their leading edge. One can see that D_{cr1} and D_{cr2} decrease very rapidly with the increase of the linear gain. This is caused by the growth of the positive net gain window at the pulse leading edge. Such growth results finally in the destruction of the pulses, as is illustrated by Fig. 13 where the phase portraits of ML regime are shown for different values of the noise power. Therefore, unlike the Q-switching bifurcation which occurs below the trailing edge instability boundary, the mechanism of the pulse breakup above the leading edge instability threshold has rather stochastic than dynamic nature.

CONCLUSION

We have derived and studied analytically and numerically a model for passive ML—a set of three differential equations with time delay (21)–(23). Near the lasing threshold, using the approach described in Refs. [31,32], Eq. (21) can be re-

duced to a partial differential equation of Ginzburg-Landau type. This reduction reveals the connection between our DDE model and Haus master equation. An important feature of our model is, however, that, unlike the Haus master equation, it does not assume small gain and loss per cavity round trip, low saturation, and infinitely broad spectral bandwidth. Such assumptions (especially the small-gain and -loss approximation) are hardly satisfied for semiconductor lasers. The only assumptions we adopt concern Lorentzian line shape of spectral filtering and ring cavity geometry. The latter approximation seems to be quite reasonable, at least for qualitative consideration of ML, unless colliding pulse ML devices are considered.

Being more general than the models proposed by New and Haus, our model includes both of them as particular limits. In the limit of infinite bandwidth of the spectral filtering element which is equivalent to the slow absorber approximation it allows analytical description, which is valid in the case of large gain and loss per cavity round trip. In particular, this refers to the pulse background instability boundaries shown in Fig. 4, and the condition (35) which gives a generalization of the well-known ML condition $s>1$. According to our results, in the parameter range typical of semiconductor lasers, background instability boundaries of ML pulses can be quite well approximated using the generalization of New's approach described in Sec. II C.

Equations (21)–(23) can be easily simulated using standard codes developed for the solution of delay differential equations. Numerical results obtained with the help of these equations are in a qualitative agreement with the experimental data. We have found that in a ring laser the shortest pulses with the highest peak powers are observed in the case when linewidth enhancement factors in gain and absorbing sections are equal to each other. Decreasing α_g below α_q results in the decrease of the pulse peak power and the increase of the pulse width. On the other hand, for $\alpha_g>\alpha_q$ a mechanism of the ML regime breakup associated with the transition from regular ML pulsations to a chaotic regime via intermittency has been observed. We have found that for nonzero linewidth enhancement factors this latter mechanism is quite general, like the known mechanisms associated with the Q-switching instability and the transitions to multiple ML regimes. Stable ML pulses with positive net gain at the leading edge have been revealed in a certain laser parameter range. Such pulses do not satisfy New's background stability criterion. A quantitative approach to the description of their sensitivity to noise is proposed in Sec. IV.

The delay differential model described in this paper can be modified to study active and hybrid ML or to take into account such additional physical effects observed in semiconductor lasers as, for example, fast nonlinearities associated with intraband relaxation processes. Moreover, under certain approximations our model can be generalized to the case of linear cavity laser design. This will be a subject of future work.

ACKNOWLEDGMENTS

We are grateful to U. Bandelow, A. Huber, B. Hüttl, R. Kaiser, G. Kozyreff, M. Nizette, D. Rachinskii, M. Radziunas, K. Schneider, E. Viktorov, M. Wolfrum, and S. Yanchuk for useful discussions and comments. We would also like to thank T. Erneux for providing us with a copy of his paper prior to its publication. A.G.V. was supported by the Terabit Optics project.

[1] P. Vasil'ev, *Ultrafast Diode Lasers: Fundamentals and Applications* (Artech House, Boston, 1995).
[2] H. Haus, IEEE J. Quantum Electron. **11**, 736 (1975).
[3] G. H. C. New, IEEE J. Quantum Electron. **10**, 115 (1974).
[4] H. A. Haus, C. Shank, and E. Ippen, Opt. Commun. **15**, 29 (1975).
[5] F. Kärtner, I. Jung, and U. Keller, IEEE J. Sel. Top. Quantum Electron. **2**, 540 (1996).
[6] F. Kärtner, J. A. der Au, and U. Keller, IEEE J. Sel. Top. Quantum Electron. **4**, 159 (1998).
[7] H. Haus, IEEE J. Sel. Top. Quantum Electron. **6**, 1173 (2001).
[8] E. Avrutin, J. Marsh, and E. Portnoi, IEE Proc.: Optoelectron. **147**, 251 (2000).
[9] R. Paschotta and U. Keller, Appl. Phys. B: Lasers Opt. **73**, 653 (2001).
[10] A. Vladimirov, D. Turaev, and G. Kozyreff, Opt. Lett. **29**, 1221 (2004).
[11] B. Tromborg, H. Lassen, and H. Olesen, IEEE J. Quantum Electron. **30**, 939 (1994).
[12] U. Bandelow, M. Radziunas, J. Sieber, and M. Wolfrum, IEEE J. Quantum Electron. **37**, 183 (2001).
[13] G. P. Agrawal and N. A. Olsson, IEEE J. Quantum Electron. **25**, 2997 (1989).
[14] V. B. Khalfin, J. M. Arnold, and J. H. Marsh, IEEE J. Sel. Top. Quantum Electron. **1**, 523 (1995).
[15] K. Ikeda, Opt. Commun. **30**, 257 (1979).
[16] K. Ikeda, H. Daido, and O. Akimoto, Phys. Rev. Lett. **45**, 709 (1980).
[17] G. L. Gurevich, Izv. Vyssh. Uchebn. Zaved., Radiofiz. **13**, 1019 (1970).
[18] G. L. Gurevich and Y. I. Khanin, Zh. Tekh. Fiz. **40**, 1566 (1970).
[19] Y. I. Khanin, *Fundamentals of Laser Dynamics* (Fizmatlit, Moscow, 1999).
[20] J. Palaski and K. Lau, Appl. Phys. Lett. **59**, 7 (1991).
[21] J. Chen, H. Haus, and E. Ippen, IEEE J. Quantum Electron. **29**, 1228 (1993).
[22] K. Engelborghs, T. Luzyanina, and G. Samaey, Department of Computer Science, K. U. Leuven, Leuven, Belgium, Technical Report No. TW-330, 2001 (unpublished).
[23] N. Guglielmi and E. Hairer, Computer Code RADAR5 (2000).
[24] T. Kolokolnikov, T. Erneux, N. Joly, and S. Bielawski (unpublished).
[25] S. Yu, T. F. Krauss, and P. J. R. Laybourn, Opt. Eng. **37**, 1164 (1991).
[26] J. P. Hohimer and G. A. Vawter, Appl. Phys. Lett. **63**, 1598

(1993).
[27] J. L. A. Dubbeldam, J. A. Leegwater, and D. Lenstra, Appl. Phys. Lett. **70**, 1938 (1997).
[28] J. M. Catherall and G. H. C. New, IEEE J. Quantum Electron. **QE-22**, 1593 (1986).
[29] J. M. Catherall, G. H. C. New, and P. Radmore, Opt. Lett. **7**, 319 (1982).
[30] G. H. C. New, Opt. Lett. **15**, 1306 (1990).
[31] G. Giacomelli and A. Politi, Phys. Rev. Lett. **76**, 2686 (1996).
[32] S. A. Kashchenko, Computational Mathematics and Mathematical Physics **38**, 443 (1998); E. V. Grigorieva, H. Haken, S. A. Kashchenko, and A. Pelster, Physica D **125**, 123 (1999).